INSIGHT INTO THE MICROSTRUCTURE OF FSW TI STABILIZED SUPERMARTENSITIC STAINLESS STEEL

Julian David Escobar [1,2], Paulo Roberto Mei [1], Antonio J. Ramirez [1,2]

[1] School of Mechanical Engineering, University of Campinas – FEM - Unicamp, Campinas, SP, 13083-860, Brazil.

[2] Brazilian Nanotechnology National Laboratory - LNNano - CNPEM, P.O. Box 6192, Campinas, SP, 13083-970, Brazil.

Carbide precipitation during multipass arc welding, hardness increments by the presence of as-welded martensite (M), and δ ferrite precipitation are critical factors for sensitization and stress corrosion cracking (SSC) in supermartensitic stainless steels (SMSS). Nevertheless, most of these detrimental effects can be avoided by using single pass welding procedures, such as friction stir welding (FSW). During this process, welding occurs inside the solid state monophasic γ field, and therefore, there is neither δ ferrite transformation nor excessive carbide precipitation at the heat affected zone (HAZ). FSW of previously tempered 12Cr-6Ni-2Mo-0.13Ti SMSS plates of 500 x 100 x 18 mm was performed in a dedicated system using 300 RPM, 100 mm.min^{-1}, and a normal force of 50 kN. Three heat affected zones were identified, regarding the five reported by arc welding. The HAZ i and ii (high temperature) were not found, completely suppressing the delta ferrite precipitation. The HAZ iii (fully austenitized) consisted of fresh martensite. The HAZ iv (partially austenitized) consisted of a mixture of fresh martensite, tempered martensite and reversed austenite.

julian.escobar@lnnano.cnpem.br – DEMA/FEM/UNICAMP, CEP 13089-970, Rua Mendeleiev, s/n - Cidade Universitaria "Zeferino Vaz" Barao Geraldo Campinas, Sao Paulo, Brazil. (55)(19)35175085

antonio.ramirez@lnnano.cnpem.br - Brazilian Nanotechnology National Laboratory LNNano - CNPEM, P.O. Box 6192, 13083-970, Campinas, Sao Paulo, Brazil. (55)(19)35183108

pmei@fem.unicamp.br – DEMA/FEM/UNICAMP, CEP 13089-970, Rua Mendeleiev, s/n - Cidade Universitaria "Zeferino Vaz" Barao Geraldo Campinas, Sao Paulo, Brazil. (55)(19) 35213322

1. Introduction

Supermartensitic stainless steels are used by the oil and gas industry as OCTG materials. Carefully designed thermomechanical processes are used to

keep low hardness (< 281 HV) [1, 2], adequate fracture toughness (150 J at -50 °C) [3, 4], moderate corrosion resistance in environments containing CO_2 and Cl^- [5], and yield strength above 500 MPa to represent a cost benefit over duplex stainless. The former characteristics are strongly influenced by an adequate distribution of finely dispersed MC carbides and reversed austenite (γ_{rt}) in a tempered martensite matrix (α'), in absence of delta ferrite precipitation (δ ferrite). However, inadequate welding procedures in SMSS can cause detrimental microstructural modifications, increasing hardness in the welded zone (WZ), and precipitating both δ ferrite and carbides at the HAZ, promoting stress corrosion cracking problems [6]. Additionally, formation over 10%vol of δ ferrite, in a fresh martensite matrix causes drastic increments of the ductile-fragile temperature transition [3]. Typically, 4 HAZs have been reported after arc welding [7]. The HAZ i (heated over A_{c5}) is formed by a fully δ ferrite microstructure. HAZ ii (heated between A_{c4} and A_{c5}) consists of a coarse grained biphasic δ ferrite + fresh martensite region. The HAZ iii (fully austenitized) contains fresh martensite. The HAZ iv (partially austenitized) involves a mixture of fresh martensite and base metal microstructure.

Friction Stir Welding (FSW) is a solid-state deformation process developed at the TWI Institute in Cambridge. It subjects the material to intense and localized plastic deformation at intermediate temperature, resulting in a fine microstructure composed by recrystallized grains [8, 9]. In FSW, a tool rotates at high speed and is plunged into the pieces to be joined and after a dwell time it starts to travel along the direction of interest. The tool generates frictional and strain hardening heat which softens the material, and thus, it can be mechanically deformed around the tool. The simultaneous rotational and translation motions of the tool during FSW generate an asymmetric zone with respect to the processing direction. The side of the zone on which the rotational motion of the tool coincides with the travel direction is called "advancing side (AS)." The opposite one is the "retreating side (RS) [10].

Due to the lower temperatures involved in FSW, it is possible to suppress the detrimental effects of the as-welded microstructure, the precipitation of δ ferrite, and the excessive grain coarsening at the HAZ. Moreover, multipass welding procedures can be avoided. Despite these advantages, little research has been conducted on Friction Stir Welding of SMSS, being the contribution of Steel (2005) [11] the most important publication to date. In the present investigation, quenched and tempered plates of UNS S41426 SMSS were joined by FSW in order to study the variation in microstructure, hardness and phase fractions.

2. Experimental Procedure

2.1 Base metal

According to the chemical composition shown in table 1, this is a highly alloyed SMSS stabilized with titanium. Titanium additions decrease the carbon and nitrogen contents in solid solution, delaying the precipitation of chromium and molybdenum carbides, enhancing ductility and weldability, and controlling hardness at the HAZ [6, 12, 13]. The as-received material was delivered as plates of 18 mm x 50 mm x 100 mm in the hot forming condition (hot rolled and annealed), and then subjected to quenching and intercritical tempering at 620

°C during 2 hours. After heat treatments, the material showed a mixture of finely dispersed Ti (C, N) particles and reversed austenite (γ_{rt}) in a tempered martensite matrix (α').

Throughout this work, γ is used to arbitrarily refer to the austenitic phase, and γ_{rt} is the percentage of reversed austenite present at room temperature after cooling from an intercritical tempering.

Table 1. Chemical composition (wt-%) of a UNS S41426 Supermartensitic Stainless Steel.

C	N	Si	Mn	P	S	Ni	Cr	Mo	Cu	Ti	V
0,024	0,0129	0,26	0,48	0,027	0,002	5,9	12,02	1,93	0,09	0,13	0,04

2.2 Friction Stir Welding

The FSW was performed parallel to the rolling direction, using a dedicated TTI FSW, which allows position and force control. FSW of previously tempered SMSS plates of 500 x 100 x 18 mm was performed using 300 RPM and 100 mm.min^{-1}, and a controlled normal force of 50 kN. A threaded conical shape, 9.25 mm long pin and convex threaded shoulder PCBN tool with metallic matrix and 40%vol W-Re (25% Re) was used. An argon atmosphere was introduced through a gas cup around the tool at a flow rate of 1.68 m^3.h.

2.3 Microstructural characterization

After FSW, samples were extracted from the cross section, perpendicular to the welding direction. The metallographic preparation consisted in grinding and polishing up to 0.25 µm particle size diamond paste. Samples were examined by LOM and SEM after etching with Vilella's reagent (60 to 120 seconds at room temperature). An Olympus microscope with a PAXCam digital camera attached to it was used for the optical microscopy performed in this study. The scanning electron microscope analyses were carried out using a FEI Quanta 650FEG. Vickers microhardness was performed through a LECO® microindentation hardness tester using a load of 1.96 N (200 gf) for 15 s. The presence of reversed austenite, before and after FSW was measured using a Panalitical X'pert Pro diffractometer, with Co Kα radiation operated at 40 kV and 45mA. Localized diffraction tests were conducted in the range of 40° to 130°, using a beam diameter of 500 µm, a step size of 0.019° (2θ) and a dwell time of 941.7 s per step. Due to the mechanical instability of the γ_{rt} phase, diffracting faces were sanded and polished to 1 µm to minimize surface deformation [3, 14].

3. Results and discussion

3.1 Microstructural characterization at the stirred zone

The microstructure of the welded zone can be classified into three different regions including the base metal (BM), which is unaffected by the process, the heat affected zone (HAZ) and the stir zone (SZ). Additionally, these regions can show distinct characteristics on the AS and the RS since the

FSW produces an asymmetrical distribution of friction and deformation in the welded joint [10]. The thermomechanically affected zone (TMAZ) was not clearly observed in this case due to the allotriomorphic transformation from γ to M, both in the AS and RS. Austenite has a preference to dynamically recrystallize and as the involved temperatures at the SZ are typically above 1000 °C [15], the formation of M at the equiaxed prior-austenitic grains is expected.

Figure 1a shows the macro etching of the FSW joint. As can be seen in figure 1i, the base metal is formed by a α' matrix with little contents of Ti (C, N) particles, finely dispersed γ_{rt} and M. Phase quantification analysis by XRD evidenced 13 ± 1 %vol γ_{rt}, and around 20%vol of M, resulting from the martensitic transformation of the less stable γ after cooling from intercritical temperings at 625 ± 5 °C [16]. Figures 1b and 1d show the upper (SZ-U) and lower (SZ-L) regions inside the SZ. A fully M microstructure can be observed. Hence, through a more detailed analysis by SEM (figure 1c, e), it is possible to notice the presence of degenerated α' needles. This evidence suggests that, regardless the fully austenitization process, the material was subjected to a quick thermomechanical process where time is not enough to cause a complete dissolution of α' needles. However, XRD analysis shown in figure 1g, evidence a complete dissolution of γ_{rt} after FSW. As the retention of γ_{rt} depends on the stabilization process through diffusion of γ-stabilizing elements during intercritical temperings [14], it is expected a complete γ to M transformation after cooling from A_{c4} temperature. The SZ-U region is subjected to a thermomechanical process in higher temperature due to the influence of the frictional heat produced by the tool shoulder. Thus, the SZ-L region suffers a colder dynamic recrystallization process, resulting in grain refinement [17, 18].

The advancing side is known as a chaotic flow region due to asymmetry in temperature and strain rate. Therefore, it is more probable to find defects within this region due to improper material flow [19, 20]. Evidence of plastic deformation can be observed in figure 1a, at the SZ-L AS region, as white lines along the interface. Advancing (SZ-AS) and Lower (SZ-L) side Stir Zones showed in figure 1f and j, respectively, evidenced a remarkable grain size refinement (500 nm to 1 μm) and fine grain boundary carbide precipitation (around 200 nm). More details can be seen by SEM images (figure 1h and k, respectively).

In SMSS, Ti is added to delay the precipitation of $M_{23}C_6$, M_2C e M_7C_3, promoting the formation of MC, and reducing hardness peaks after welding. Nevertheless, in this case, Ti (C, N) particles show a detrimental effect, acting as barriers to the material flow. Figure 1h shows a detailed study of the microdefects found at the SZ-AS. Little presence of coarse Ti (C, N) particles can be noticed, and a high density of carbide-shaped voids was evidenced. This can be explained due to the specific thermomechanical conditions at the SZ-AS. Coarse Ti (C, N) particles are no longer transported but broken, and dispersed along the flowing fronts during stirring, ending at the advancing side interface. These particles could have been removed from the matrix during the metallographic preparation, leaving geometrically coincident voids. Therefore, there is a high density of defects along the grain and flow line boundaries. Additionally, as the temperature is not enough to balance strain hardening, and these particles are barriers to deformation, conditions are given to further carbide precipitation along the grain boundaries, as shown in figures 1h and k.
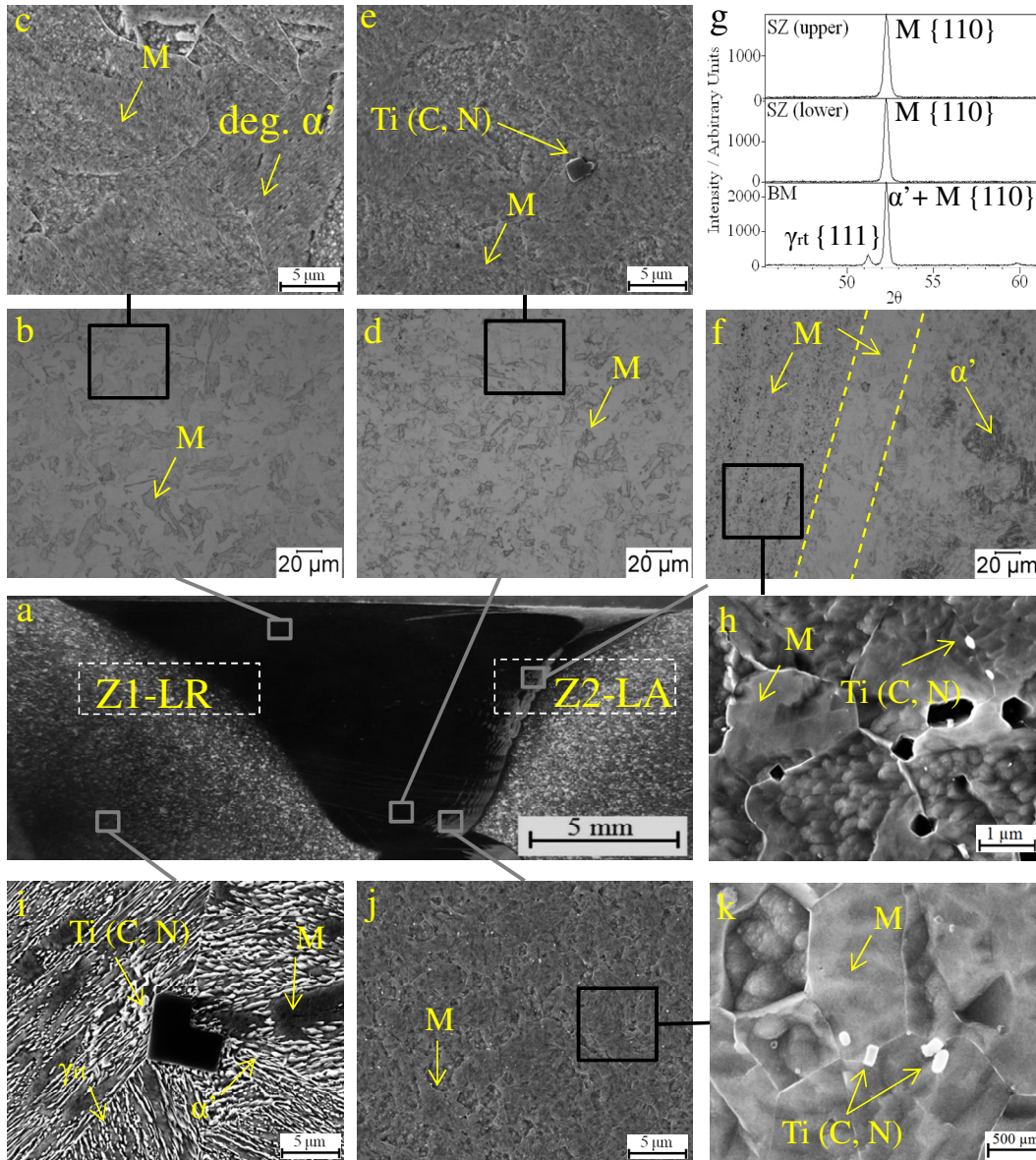
Figure 1. Microstructural characterization of a quenched and tempered 12CR-6Ni-2Mo-0.13Ti SMSS after FSW. a) Macroetching, b) SZ-U, c) detail of the SZ-U, d) SZ-L, e) detail of the SZ-L, f) SZ-AS, g) XRD analysis at the SZ and BM, h) detail of the SZ-AS, i) BM, j) SZ-L AS, k) detail of the SZ-L AS. Deg: degenerated, SZ: stir zone. U: upper, L: lower, AS: advancing side, RS: retreading side. M: fresh martensite, α': tempered martensite, Ti (C, N) titanium carbonitrides. Villela's reagent.

3.2 Microstructural characterization at the heat affected zones

The microstructural modifications due to the thermal cycle at the AS and RS of the heat affected zones, indicated in figure 2a as Z1 and Z2, respectively, were studied. Three different heat affected zones can be identified in both the RS (figure 2a) and AS (figure 2b). The microstructural evolution at the RS is shown in figures 2b to e. A detailed microstructural characterization at the AS is presented in figures 2f to i. Figure 2b shows the BM microstructure, composed

by α' and 16%vol of γ_{rt}, measured by localized XRD. Grain boundaries were highlighted in white for comparison purposes (figure 2i).
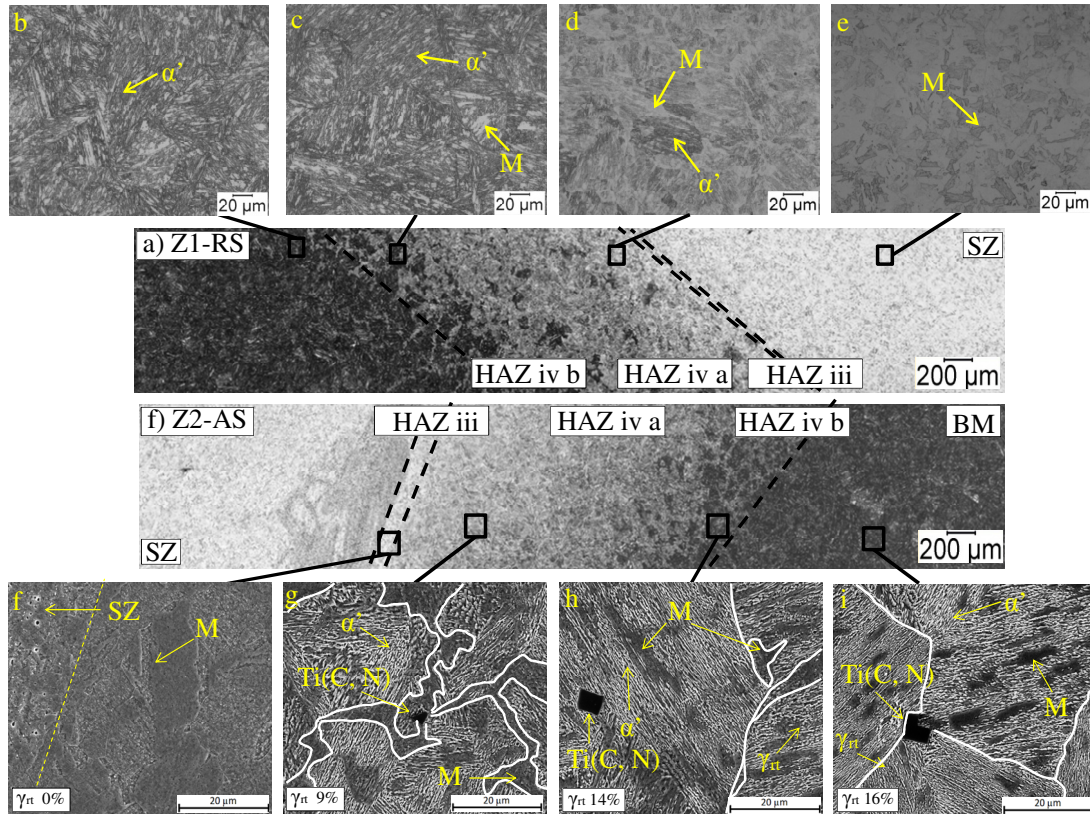

Figure 2. Detail of the heat affected zones of a quenched and tempered 12CR-6Ni-2Mo-0.13Ti SMSS after FSW. a) Advancing side, and their respective regions (LOM): b) base metal, c) HAZ iv b, d) HAZ iv a, e) stir zone; f) Retreading side and its respective regions (SEM): g) HAZ iii, h) HAZ iv a, h) HAZ iv b, i) HAZ iv a, j) base metal. M: martensite, M': tempered Martensite, Ti (C, N) titanium carbonitrides. Villela's reagent. Slight

The first microstructural modification was evidenced at the HAZ iv b, defined as the region where the material suffered a quick intercritical tempering at low temperature. Heating slightly above A_{c1} causes decomposition of α' into γ and γ_{rt} into γ; and therefore, martensitic transformation during cooling, reducing γ_{rt} to 14%vol. As described by Bilmes [21] and Leem [14], austenite can nucleate both at grain boundaries and between the α' needles. Consequently, after cooling, fresh martensite is expected to appear at these sites, as detailed in figure 2c. The α' matrix is still visible and a slight reduction in the γ_{rt} was noticed, as detailed in figure 2h.

Moving towards the SZ, the HAZ iv a can be identified. Although the phase transformations also occur at the intercritical region, a higher fraction of γ is present, owing to an increased peak temperature and a faster α' to γ and γ_{rt} to γ decomposition. After cooling, a higher M fraction was present, evidenced in figure 2d as the clearer phase. Figure 2g shows a closer view to this region. Fresh martensite between α' needles and mainly along the grain boundaries can be identified. As described by Karlsen [22], these are the places where γ_{rt} retention occurs, therefore a reduced γ_{rt} percentage to 9%vol can be noticed.

HAZ iii, defined as the region where the base metal was heated into the fully austenitic region, is shown in figure 2f. After cooling, austenitic was transformed into fresh martensite, resulting in a microstructure similar to the SZ shown in figure 2e. A complete γ_{rt} decomposition was observed.

3.3 Hardness modifications after FSW

Figure 3 shows hardness measurements at the cross section after FSW. The lowest hardness (283 ± 5 $HV_{0.2/15}$), was found at the BM due to a tough microstructure consisting on α' and γ_{rt}. When compared to the BM, The HAZ iv b shows the first hardness increment (310 ± 5 $HV_{0.2/15}$) due to the partial martensitic transformation after cooling. At the HAZ iv a, the material was heated to a higher intercritical temperature, showing higher hardness (335 ± 4 $HV_{0.2/15}$), when compared to the SZ (325 ± 7 $HV_{0.2/15}$). This is due to a higher presence of M and to secondary hardening owing to carbide precipitation. In quenched and tempered SMSS, alloyed with molybdenum, there is a tendency to precipitate $M_{23}C_6$ and mainly M_2C carbides after reheating cycles in temperatures between 620 °C and 680 °C [13, 21]. However, secondary hardening can be largely avoided by using pre-heating temperatures during welding. The ZTA iii and the SZ showed a similar hardness value of 330 $HV_{0.2/15}$ due to the presence of a fully M microstructure. As expected, the highest hardness of the cross section was found at the SZ-AS (360 ± 6 $HV_{0.2/15}$) due to the combined effect of grain refinement, carbide precipitation and strain hardening.
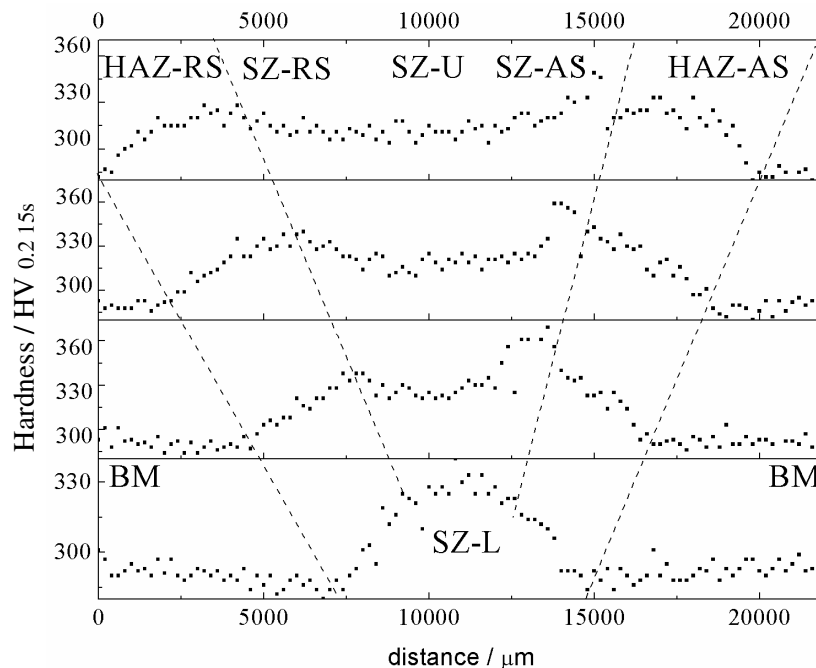

Figure 3. Hardness measurements from 4 horizontal positions at the cross section of a quenched and tempered 12CR-6Ni-2Mo-0.13Ti SMSS, after FSW. U: upper, L: lower, AS: advancing side, RS: retreading side.

4. Conclusions

Stir zone

- At the upper region of the SZ, it was found lath martensite (10 µm) and finely dispersed Ti (C, N) particles (2 µm). At the bottom of the SZ, it was found a more refined grain size (about 1 µm), as well as Ti (C, N) particles. δ ferrite precipitation wasn't observed and all reversed austenite was decomposed and transformed to fresh martensite during cooling.
- The average hardness of the SZ was 330 $HV_{0.2/15}$, higher than the base metal (280 $HV_{0.2/15}$), as a consequence of the dynamic recrystallization process and the γ to M transformation during cooling. The maximum hardness value (380 $HV_{0.2/15}$) was found within the mixed zone at the SZ-AS interface due to a high density of defects, evidence of strain hardening and carbide precipitation.

Heat affected zones

- The high temperature heat affected zones HAZ i (fully δ ferrite) and HAZ ii (coarse M and δ ferrite) were not found after FSW.
- Only low temperature HAZ were found after FSW. HAZ iii (fully austenitized) was composed of M and Ti (C, N) particles. HAZ iv a (partially austenitized at high temperature) evidenced mainly M, and little presence of α' and γ_{rt}. HAZ iv b (partially austenitized at low temperature) showed mainly a α' matrix with presence of M and little decomposition of γ_{rt}.
- It was observed hardening for all regions of the HAZ relative to the base metal. Upon reaching intercritical austenitization at low temperature, HAZ iv b evidenced hardening by γ to M transformation, showing an average hardness of 320 $HV_{0.2/15}$. At higher intercritical austenitization temperatures, a higher M fraction along with secondary hardening was observed, resulting in 350 $HV_{0.2/15}$.

6. References

1. NACE International. ANSI/NACE/MR0175/ISO15156-3: Petroleum and natural gas industries - Materials for use in H2S-containing environments in oil and gas production, 2010.
2. RAMIREZ, J.E. Weldability Evaluation of Supermartensitic Stainless Pipe Steels. Welding Research, v. 86, May 2007.
3. Carrouge, D. Phase transformations in welded supermartensitic stainless steels. Doctoral thesis - University of Cambridge. 185p. 2002.
4. SILVA, G.F.; TAVARES, S.S.M.; PARDAL, J.M.; SILVA, M.R.; ABREU, H.F.G. Influence of Heat Treatments on Toughness and Sensitization of a Ti-alloyed Supermartensitic Stainless Steel. Journal of Material Science, v.46, p. 7737-7744, 2011.
5. KONDO, K.; UEDA, M.; OGAWA, K.; AMAYA, H.; HIRATA, H.; TAKABE, H. Alloy Design of Super 13 Cr Martensitic Stainless Steel (Development of Super 13 Cr Martensitic Stainless Steel for Line Pipe). In: Supermartensitic Stainless Steels '99'. In: Anais… p. 11–18, Belgium, 1999.

6. WOOLLIN, P. Welding Supermartensitic Stainless Steels for Corrosive Service. Stainless Steel World Conference, Maastricht, Netherlands, 6-8 november, 2007.

7. WOOLLIN, P.; CARROUGE, D. Heat affected zone microstructures in supermartensitic stainless steel. Proceedings in: Supermartensitic Stainless Steels 2002. Belgium, 2002. Paper 027.

8. A. Chabok, K. Dehghani. Dependence of Zener parameter on the nanograins formed during friction stir processing of interstitial free steels. Materials Science and Engineering: A, Volume 528, Issues 13–14, 25 May 2011, Pages 4325–4330

9. Sterling, C. Effects of friction stir processing on the microstructure and mechanical properties of fusion welded 304L stainless steel. MSc thesis, Brigham Young University, 2004

10. R.S. Mishra, M.V Mahoney. "Friction Stir Welding and Processing", Ohio: ASM International, 2007, 360p.

11. STEEL, R. J.; LILJEBLAD, L.E.; PACKER, S.M.; NELSON, T.W.; SANTOS, J.F. Friction Stir Welding of 12Cr-7Ni-2Mo Supermartensitic Stainless Steel. Stainless Steel World Conference, P5039.4, 2005.

12. RODRIGUES, C.A.D.; LORENZO, P.L.D.; SOKOLOWSKI, A.; BARBOSA, C.A.; TREMILIOSI, F.; ROLLO, J.M.D.A. Titanium and molybdenum content in supermartensitic stainless steel. Materials Science and Engineering A, v.460-461, p. 149-152, 2007.

13. LADANOVA, E.; SOLBERG, J.K.; ROGNE, T.; Carbide precipitation in HAZ of multipass welds in titanium containing and titanium free supermartensitic stainless steels part 1 – Proposed precipitation mechanisms. Corrosion Engineering, Science and Technology, v. 41, p. 143-160, 2006.

14. LEEM, D.; LEE, Y.; JUN, J.; CHOI, C. Amount of retained austenite at room temperature after reverse transformation of martensite to austenite in an Fe-13%Cr-7%Ni-3%Si martensitic stainless steel. Scripta Materialia, v. 45, p. 767-772, 2001.

15. SANTOS, T.F.A. Avaliação microestrutural e de desempenho de juntas soldadas de aços inoxidáveis duplex por atrito com pino não consumível. 2012. Tese (Doutorado) – Universidade Estadual de Campinas, Campinas. 189 p.

16. ESCOBAR, J.D.; FARIA, G.; WU, L.; MEI, P.R.; RAMIREZ, A.J. In-situ study of reverted austenite and TRIP effect of a Ti stabilized supermartensitic stainless steel. Stainless Steel World Conference, 13-14 November 2013, Maastricht, The Netherlands.

17. Sato, Y.S. Microstructure and mechanical properties of friction stir welded SAF 2507 super duplex stainless steel, Materials Science and Engineering A ,v. 397, p.376-384, 2005.

18. T. Saeid, A. Abdollah-zadeh, H. Assadi, F. MalekGhaini. Effect of friction stir welding speed on the microstructure and mechanical properties of a duplex stainless steel Materials Science and Engineering A 496 (2008) 262–268.

19. KUMAR, K.; KAILAS, S.V. The role of friction stir welding tool on material flow and weld formation. Materials Science and Engineering A, v. 485, p.367-374, 2008.

20. ELANGOVAN, K.; BALASUBRAMANIAN, V. Influences of pin profile and rotational speed of the tool on the formation of friction stir processing zone in AA2219 aluminium alloy. Materials Science and Engineering A, v. 459, p. 7-18, 2007.

21. BILMES, P.D.; SOLARI, M.; LLORENTE, C.L. Characteristics and Effects of Austenite Resulting from Tempering of 13Cr-NiMo Martensitic Steel Weld Metals. Materials Characterization, v. 46, p. 285-296, 2001.

22. KARLSEN, M.; HJELEN, J.; GRONG, Ø.; RØRVIK, G.; CHIRON, R.; SCHUBERT, U. The stability of retained austenite in supermartensitic stainless steel (SMSS) examined by means of SEM/EBSD. In: EMC 2008 14th European Microscopy Congress 1–5 September 2008, Aachen, Germany, pp 561-562, 2008.